UCRL-84684 Rev. I
PREPRINT

CONF-8009132--1(Rev 1)
CONF-801119--3(Rev 1)

LASER IRRADIATION OF DISK TARGETS AT 0.53-μm WAVELENGTH

M. C. MEAD, E. M. CAMPBELL, K. G. ESTABROOK,
R. E. TURNER, W. L. KRUER, P. H. Y. LEE,
B. PRUETT, V. C. RUPERT, K. G. TIRSELL,
G. L. STRADLING, F. ZE, C. E. MAX, AND M. D. ROSEN

This report is a written account of work presented at the 14th European Conference on Laser Interaction with Matter, Palaiseau, France, September 15-19, 1980, and at the 22nd Annual Meeting of the Division of Plasma Physics, San Diego, CA, November 10-14, 1980.

January 26, 1981

Laser Irradiation of Disk Targets at 0.53 μm Wavelength

W. C. Mead, E. M. Campbell, K. G. Estabrook, R. E. Turner,
W. L. Kruer, P. H. Y. Lee, B. Pruett, V. C. Rupert, K. G. Tirsell,
G. L. Stradling, F. Ze, C. E. Max, and M. D. Rosen

Lawrence Livermore National Laboratory,
Livermore, California 94550

ABSTRACT

We present results and analysis for laser-irradiations of Be, CH, Ti, and Au disk targets with 0.53 μm light in 3-35 J, 600 ps pulses, at nominal intensities from 3×10^{13} to $\sim 4 \times 10^{15}$ W/cm^2. The measured absorptions are higher than observed in similar 1.06 μm irradiations, and are largely consistent with modeling which shows the importance of inverse bremsstrahlung and Brillouin scattering. Observed red-shifted back-reflected light shows that Brillouin is operating at low to moderate levels. The measured fluxes of multi-keV x-rays indicate low hot-electron fractions, with temperatures which are consistent with resonance absorption. Measurements show efficient conversion of absorbed light into sub-keV x-rays, with time-, angular-, and spatial-emission distributions which are generally consistent with non-LTE modeling using inhibited thermal electron transport.

---

*Work performed under the auspices of the U.S. Department of Energy by the Lawrence Livermore National Laboratory under Contract No. W-7405-ENG-48.

I. Introduction

In this report, we present highlights of the wavelength-scaling experiments performed on ARGUS to date.[1] We report new results for irradiations with 0.53 μm, 600 ps pulses at $\sim 10^{13}$-10^{15} W/cm^2, discussing the results in some detail in terms of hydrocode simulations and theory. Analogous experiments are in progress at 0.35 and 1.06 μm, however, results from these experiments are not yet available. Where appropriate, we will call upon previous 1.06 μm experiments and calculations which have somewhat different irradiation parameters. This will enable us to see the more evident wavelength-scaling trends, although improved quantitative reliability must await completion of the entire set of scaling experiments. The results to date are very interesting: we find considerable support for theoretical predictions, and several areas where improved understanding is needed.

The report is organized as follows. In Sec. II the important features of the LASNEX computer-code modeling used to simulate these experiments are reviewed. Section III presents LASNEX wavelength-scaling calculations and discusses some of the major trends of using shorter-than-1-μm irradiation wavelengths. Section IV gives the experimental irradiation conditions. Results of the experiments and simulations are then presented: absorption and scattering (Sec.

V), multikilovolt x-rays and suprathermal electrons (Sec. VI), and sub-kilovolt x-ray emission (Sec. VII). The role of electron conduction is discussed in Sec. VIII. Finally, the key results are summarized in Sec. IX.

II. Features of the LASNEX Modeling

Extensive computer simulations of these wavelength-scaling experiments have been performed using the LASNEX[2] Lagrangian hydrodynamics code to solve the equations for the bulk evolution of the laser-target interactions. The LASNEX modeling used for the calculations presented here is largely consistent with that employed for many previous simulations of experiments.[3,4,5] We mention here some of the key features and discuss their importance to the present calculations.

Most calculations have been performed in 1-dimensional spherical geometry, using a radius of curvature which is equal to twice the laser spot diameter. These pseudo-two-dimensional calculations have been compared in detail with several full two-dimensional calculations. We find that the pseudo-2-D calculations are quite adequate for most of the plasma characteristics and diagnostic properties of interest in these experiments.

The absorption model includes classical absorption due to inverse bremsstrahlung, collective absorption via resonance absorption, and, most recently, a model for stimulated Brillouin back-scatter. The

ponderomotive force is included, but is found to be negligible compared with thermal plasma pressures resulting from localized energy-deposition and ablation near the critical surface.

The inverse bremsstrahlung modeling used for calculations presented in this work uses the classical absorption cross-section. We did not include the non-linear opacity reduction reported by Langdon.[6] However, we have estimated the expected effect: a reduction of the inverse bremsstrahlung absorption opacity by a factor of ~0.6 for the gold disk targets at 2×10^{15} W/cm^2 (reducing absorption by ~10% for this case), and considerably less change elsewhere. We believe other absorption mechanisms which are also neglected in the modeling, such as short-wavelength ion turbulence,[7] could approximately compensate for the moderate non-linear reduction of inverse bremsstrahlung calculated for these plasmas. In addition, the strong dependence of the inverse bremsstrahlung opacity on the plasma density, temperature, and ionization state leads to significant quantitative uncertainty in the model, probably larger than the omitted non-linear effects.

The model for resonance absorption[8,9] is very simple. A specified fraction (f_d) of the light reaching the critical density surface is deposited into a suprathermal electron distribution. The value of f_d can be motivated by theory or by matching observed hard x-ray fluxes. The temperature of the suprathermal-electron source is set by a semi-empirical scaling law which matches both experiments and plasma simulations.

The model has been extended recently in one major area: the 1-D absorption model now has a calculation of the level of stimulated Brillouin back-scatter.[10] The model calculates the evolution of Brillouin ion-waves based on the LASNEX-calculated plasma profiles. The backscatter fraction is then calculated from a model based on theory and plasma simulations. The backscattered light is tracked outward through the plasma and may rescatter once, a process which can become significant at the highest Brillouin levels.

The atomic physics model used for the LASNEX calculations discussed here is identical with that employed previously by Rosen, *et al.*[5] It includes a solution of the time-dependent ionization and radiation rate equations, in an average-atom approximate treatment.[11] The use of a full non-LTE model is essential for the mid- to high-Z target irradiation parameters in these experiments, since very steep density and temperature gradients are produced by the absorption near the critical surface, and the high-Z plasmas have very high radiative rates. Large errors would be made in calculating the ionization state and temperatures in the corona if LTE were artificially enforced.

The electron conduction modeling used here is the same as that used for modeling many previous experiments.[3,4,5] Thermal electrons are modeled by a single Maxwellian group, transported by flux-limited diffusion. The thermal flux limit is taken as $f_\ell = 0.03$. This provides flux-limitation at essentially the same level as the ion-acoustic turbulence model in LASNEX. A large body of evidence supports using this value for LASNEX simulations of 1.06 μm

experiments.[3,5,12] The suprathermal electrons are modeled using multigroup flux-limited diffusion with no anomalous flux limit reduction, but with fairly self-consistent electric field coupling (via $J_{tot} = 0$) to the thermal electrons.[3]

III. Wavelength Scaling Trends

Most of the advantages of using shorter wavelength lasers to drive fusion microimplosions accrue because the shorter wavelength light deposits its energy in higher plasma densities. Hence, corona temperatures (at a given intensity) are lower, and collision rates are higher. Most of the collective laser-plasma interaction effects then have higher thresholds and lower growth rates.[13] Inverse bremsstrahlung absorption becomes increasingly effective. Thus, at sub-micron wavelengths, we expect to obtain higher absorption, reduced suprathermal electron production, and higher thermal and hydrodynamic coupling efficiencies.[14]

As an example, we show in Fig. 1 a set of early LASNEX wavelength-scaling predictions. The plot shows the total absorption, the fractional absorption into suprathermal electrons by resonance absorption at the critical surface, and the conversion efficiency of absorbed energy into x-rays for gold disk target irradiations at 3×10^{14} W/cm^2, 12 J, and 600 ps. The LASNEX model used for these calculations is identical with that used to analyze previous experiments at 1.06 μm wavelength.[5] This model used a fixed resonance-absorption $f_d = 0.30$ and did not include the effects of

stimulated Brillouin scattering. A model for Brillouin back-scatter is incorporated in the more recent LASNEX calculations discussed in the remainder of this report, but it affects this modest-intensity case only slightly. The qualitative trends associated with increased collisionality are shown quantitatively by the simulations.

In Fig. 2, we show LASNEX-calculated plasma profiles for a gold disk target irradiation at 3×10^{14} W/cm^2, 25 J, and 600 ps with 0.53 μm laser wavelength. Qualitatively, the profiles are quite similar to those calculated for 1.06 μm wavelength. The temperature at the critical surface has dropped from 2.0 to 1.1 keV, and the peak temperature in the corona has decreased from 2.6 to 2.1 keV. The peak corona temperature scales as $\lambda^{0.3}$, in rough agreement with simple scaling arguments for inverse bremsstrahlung in the moderate-absorption regime.[15] At the critical surface, the temperature scales more strongly, $T_c \sim \lambda^{0.9}$, since the intensity at critical drops steeply as the light is more efficiently absorbed in the underdense plasma.

The calculations also show an increase in x-ray conversion efficiency at shorter laser wavelengths. As the laser wavelength decreases, the critical surface lies at higher density, so that more energy is carried into the high density plasma, where sub-keV x-rays are emitted most effectively.

Next, we discuss key features of the ARGUS wavelength-scaling

experiments to date in terms of LASNEX simulations and these expected trends.

IV. Experimental Irradiation Conditions

The experiments discussed here have irradiated isolated 600-μm diameter by 20-μm thick disk targets of Be, CH, Ti, and Au with 0.53 μm light from the frequency-doubled Argus Nd-glass laser. Nominal intensities of 3×10^{13}, 3×10^{14}, 2×10^{15} and $\sim 4 \times 10^{15}$ W/cm^2 were obtained at energies of 3-35 J by varying the target position with respect to the f/2 focusing lens, using spot diameters of 450 to 50 μm. Gaussian 600 ps pulses were used.

Very complete laser energy distribution measurements were made using both equivalent-plane and chamber-transmission techniques. The energy is incident on the target with RMS intensity fluctuations of a factor of 1.4-2., with 5-25 μm spatial structures. Below, we present the data in terms of "nominal" intensities, together with intensity "bars" which show the range of intensities containing 60% of the incident energy.

V. Absorption and Scattering

The results of 0.53 μm absorption measurements[1] made using the "box-calorimeter" for Be, CH, and Au disk targets at normal incidence are shown in Fig. 3. The measurements show that absorption increases

at decreasing intensity and increasing target Z, qualitatively as expected for collisional absorption by inverse bremsstrahlung.

We observe increased absorption at 0.53 μm compared with similar 1.06 μm experiments using gold disk targets. For example, the absorption measured at 3 X 10^{14} W/cm^2 is 80 ± 5% for 0.53 μm wavelength and 600 ps pulse duration, while earlier 1.06 μm experiments[5] obtained 53 ± 5% at 900 ps. The 1.06 μm absorption would probably be somewhat reduced at the shorter 600 ps pulse duration, based upon other 1.06 μm experiments and calculations. Thus, for gold disk targets at 3 X 10^{14} W/cm^2 and 600 ps, the absorption for 0.53 μm light is higher by roughly a factor of 2 than that at 1.06 μm.

Lower Z targets show significantly higher absorption at 0.53 μm wavelength, as well. Measurements for CH-disk targets irradiated at 1.06 μm, 5 X 10^{14} W/cm^2, 75 J, and 300 ps using the Cyclops laser showed 25% absorption.[4] The recent 0.53 μm experiments show again an increase of about a factor of 2 at this intensity. Short-pulse wavelength-scaling experiments performed by Amiranoff, *et al.*, exhibit similar absorption trends for low-Z targets.[16]

In the LASNEX modeling of these experiments, we reduced the amount of absorption via collective processes (f_d) in order to match the measured high-energy x-ray fluences (discussed below). Except where otherwise stated, we have used $f_d = 0.03$ throughout this work. This is considerably lower than the value (0.3) which has usually been motivated on the basis of plasma kinetic simulations of resonance

absorption[8,9] and short pulse laser-plasma interaction experiments.[3] We note that earlier work at 1.06 μm has shown similarly reduced hard x-ray fluxes.[5,17,18] A similarly reduced f_d was motivated by Rosen, *et al.*,[5] on the basis of estimates of three effects: a broad range of incidence angles, stimulated Brillouin scattering, and extended density scale lengths at the critical surface. In the present work, using f/2 optics, we find no detectable (factor of ~3) variation of the high-energy x-ray flux between incidence angles of 0° and 30°. As discussed below, we find the effects of Brillouin and extended density scale-lengths to be quite likely contributors to the reduced hot-electron levels.

We calculate significant levels of Brillouin scattering in the 2 X 10^{15} W/cm^2 beryllium disk simulations. This case has the longest gradient-lengths in the underdense plasma, and its laser intensity lies farthest above threshold. Here we calculate that 70% of the incident light is backscattered on its way to the critical surface. Of course, when the Brillouin level becomes this high, significant multiple scattering is encountered: about 30% of this Brillouin-scattered light is rereflected inward, giving a net backscatter of 50% of the incident light.

The absorptions calculated by LASNEX using $f_d = 0.03$ and nominal inverse bremsstrahlung opacity are plotted in Fig. 3, for comparison with the data. The calculations reproduce the observed behavior to within about 10-15% of the absorption. The largest errors occur for the high-intensity irradiations of beryllium targets. This is

precisely where additional collective absorption would occur if we had employed $f_d = 0.3$. We discuss this puzzle further in connection with the multi-kilovolt x-ray measurements and simulation results. For the present purposes, we reiterate that other processes could also provide the required additional 10-15% absorption: short-wavelength ion turbulence;[7] slightly increased thermal electron transport (which would make inverse bremsstrahlung more effective); or a reduction in stimulated Brillouin scatter (relative to the calculated levels, as discussed below).

Experimentally, we obtain evidence for the presence of stimulated Brillouin scatter from measurements of the spectrum of the back-reflected light.[1] We find behavior at 0.53 μm wavelength which is qualitatively similar to that seen at 1.06 μm. However, we observe striking qualitative differences between the backscatter spectra of low- and high- Z targets. The backscatter spectrum has been reported previously,[17] so here we simply note that at 3×10^{14} W/cm^2, CH disk targets show a blue-shifted plateau from -1.2 to -0.3 nm, and a peak from -0.3 to +0.1 nm, whereas the gold disk targets show mainly a single broad red-shifted peak from ~0 to +0.5 nm (wavelengths are relative to that of the incident laser light). Quantitative interpretation of these spectra and the strong Z-dependence is elusive, and remains a subject for continued effort. At present, simulations seem to imply somewhat stronger blue-shifts than are measured. This much is quite clear: the backscatter spectra show indications that Brillouin scattering is indeed operating at

significant levels in the higher-intensity irradiations, even for these relatively short scale-length plasmas.

We also observed the spectrum of reflected light near $\omega_{inc}/2$ for the 0.53 μm irradiations in order to determine a lower limit for the level of Raman scattering occuring.[18] For these plasmas, the energy observed in the wavelength band from 0.6 to 1.0 μm was less than $\sim 10^{-5}$ of the incident energy.[1] Based on the LASNEX-calculated density and temperature profiles, we estimate that the highest irradiation intensities employed in these experiments exceed the Raman side-scatter threshold by less than a factor of ~3, so these low levels seem reasonable.

The threshold for the two-plasmon decay instability[19] is about a factor of 10 lower than that for Raman side-scatter, so it is possible that some $2\omega_{pe}$ is occuring in these experiments. However, no means of isolating this process is available in the present measurements.

VI. Multi-kilovolt X-rays and Suprathermal Electrons

The fluence of multi-kilovolt x-rays has been measured to permit inferrence of the levels of suprathermal electrons generated by the laser-plasma interactions.[1] The detectors span the x-ray energy range from about 5 to 70 keV. K-edge filtered detector signals have been unfolded to determine the spectra emitted by the targets. We find shot-to-shot variations about the mean of a factor of about 2 to 3 in

fluence, but only about 20% in slope or "effective temperature" (based on the highest two channels).

The spectra measured for varying irradiation intensity and target Z are shown in Fig. 4. The high energy x-ray fluence increases dramatically with increasing irradiation intensity, as shown for gold disk targets in Fig. 4a. This has been qualitatively observed in many other experiments. (We note that the intensity modulation of the incident light affects the inferred hot-electron temperatures to some extent, however, this effect has not been considered in detail.) At 2×10^{15} W/cm^2, we observe an increase in both x-ray fluence and spectral hardness as the target Z increases, Fig. 4b, also in accord with previous 1.06 μm results.[20]

Comparing these spectra to measurements performed previously[20] using similar irradiation conditions at 1.06 μm ($3-5 \times 10^{14}$ W/cm^2, 400 J, 900 ps), we note some curvature in the 20–70 keV photon energy range. Instead of the constant exponential drop-off generally seen in this spectral regime at 1.06 μm, the spectrum from 0.53 μm irradiations shows a distinct shift in slope between adjoining x-ray channels. This qualitative feature is seen in the LASNEX simulations, although the calculated spectrum shows some quantitative departures from that measured (discussed below). The emission at intermediate photon energies in high-Z plasmas arises from heating of the thermal background electrons in the underdense plasma by efficient collisional absorption and subsequent free-bound emission. These processes are more pronounced at shorter wavelengths because the "underdense" plasma

has higher density, and hence, higher free-bound emission rates than at longer laser wavelengths.

We also have weak evidence from comparing the filter-fluorescer and K-edge detectors that the spectrum may harden further at photon energies above 70 keV. This is seen mainly in the gold disk, 3×10^{14} W/cm^2 irradiations where the hard x-ray fluences are very low and may indicate the presence of a very small amount of the $2\omega_{pe}$ instability.[19]

Order-of-magnitude estimates of the electron populations required to produce the hard x-ray emission seen here have been made assuming the radiation is produced by bremsstrahlung[21] from a Maxwellian component of the electron distribution function. The x-ray flux (in keV/keV-4π) at the photon energy equal to the hot electron temperature ($h\nu = kT_h$) is given by

$$\varphi_h \approx 6.3 \times 10^9 \, Z \, E_h \, ,$$

where Z is the atomic number of the matter in which the electrons are slowing down and E_h is the energy (in J) contained in the hot Maxwellian distribution. In this simple estimate, we neglect losses of suprathermal electron energy to hydrodynamic plasma expansion, but we generally find that these estimates agree with LASNEX calculations to within a factor of 2 to 4.

To estimate the hot electron populations for the experiments here, we must deal with the spectral curvature discussed above. We analyze a (Z-dependent) region of the spectrum which is as free as

possible of free-bound background emission, extrapolating the high-$h\nu$ fluence to $h\nu = kT_h$ using the T_h inferred from the highest two detector channels available. The results are presented in Table 1. The table entries indicate the spectral region analyzed to obtain the T_h and E_h values.

The hot electron temperatures and populations both increase as the irradiation intensity increases. The levels inferred fluctuate to some extent, but are generally quite low, less than ~1% in all cases.

The temperatures and populations at 2×10^{15} W/cm^2 for 0.53 μm wavelength irradiations are the same (within uncertainties) as observed in the cited 1.06 μm experiments[20] at 5×10^{14} W/cm^2. This is in accord with the expected behavior of heating by resonance absorption, since $I\lambda^2$, the relevant scaling parameter, is approximately the same for the two sets of experiments. We emphasize that more reliable wavelength-scaling comparisons of the suprathermal electron populations must await completion of directly comparable experiments.

The results at 2×10^{15} W/cm^2 also suggest some increase in T_h with increasing target Z, with scaling roughly as $T_h \sim Z^{0.25}$. This is consistent with scaling observed in previous 1.06 μm experiments.[20] Theoretically, this can be at least partially explained. Plasma kinetic simulations[22] suggest that the combined effects of albedo and reheating of the hot electrons nearly cancel, yielding no significant Z-dependence for the resonance-absorption T_h from these effects.

LASNEX simulations for these experiments which do not include an explicit Z-dependence in the T_h resonance absorption model do, however, show a weak Z-dependence, roughly $T_h \sim Z^{0.15}$. This results from Z-dependent conduction[23] and inverse bremsstrahlung heating rates[15] which raise the background temperature in higher-Z plasmas. The resonance absorption T_h is in turn increased by this increased background temperature. Thus, theory suggests a weaker Z-dependence than is typically observed. This discrepancy is not large nor is it clearly outside the bounds of reasonable experimental errors.

Quantitative accounting for the measured hard x-ray fluence proves too challenging for the current LASNEX absorption/hot-electron modeling. Figure 5 shows a comparison of LASNEX calculations using various f_d-values with the hard x-ray data from gold disks irradiated at 2 X 10^{15} W/cm^2, 0.53 μm. We note that all these simulations show excessive emission for intermediate photon frequencies in the 10-30 keV range. A similar discrepancy can be seen in earlier 1.06 μm experiments.[5] Best agreement with the high-energy photon spectrum is obtained using $f_d = 0.03$.

As discussed in the preceeding section, when we perform LASNEX calculations with the usual $f_d = 0.3$ (uppermost curve in Fig. 5), the calculated hard x-ray fluences are about a factor of 10 too large compared with measurements. A similar discrepancy in the hard x-ray flux was seen in short-pulse, high-intensity 1.06 μm experiments.[24] LASNEX simulations of those experiments calculated resonance-absorption values nearly equal to the chosen f_d-value, and

$f_d = 0.3$ yielded calculated x-ray fluxes considerably higher than measured.

These discrepancies would be resolved if the absorption processes are generating considerably fewer suprathermal electrons, or, perhaps if the suprathermals which are produced are confined to low density regions of the plasma so that the bremsstrahlung radiation produced is much reduced. We have found that the latter hypothesis is very difficult to support since the ratio of the radiative- to hydrodynamic- energy loss rate must be altered by a very large factor to reduce the hard x-ray emission by a factor of ~10. Using the suprathermal electron modeling of LASNEX, even with a very large (~100-fold) reduction in suprathermal transport coefficient, we are unable to adequately reduce the hard x-ray emission. Furthermore, two-dimensional calculations which include thermoelectric magnetic field generation do not show the required severe inhibition of suprathermal electron transport, so it seems difficult to provide a sufficiently strong confinement mechanism for the suprathermals. Stepping for a moment outside the LASNEX suprathermal-transport model, estimates based upon suprathermal orbiting[25] suggest that electrons would be inadequately confined to low density plasma unless the corona were considerably larger than calculated by LASNEX or by estimates based upon isothermal expansion. Thus, for this work, we have adopted the reduced resonance-absorption hypothesis, using $f_d = 0.03$. We suggest that resonance absorption may be efficient only for ultra-short laser pulses (say, $\tau_L < 60$ ps at $\sim 10^{15}$ W/cm^2 and 1.06 μm) since slower rise-times create longer density gradients as the plasma

develops. This longer scale-length could in turn make the resonant region inaccessible,[9] reducing the momentum deposited by hot-electrons ejected down the density gradient by resonance absorption, and further inhibiting self-steepening at the critical surface. Quantitative estimates suggest that a scale-length at the critical surface of several microns, which is long enough to inhibit resonance absorption, could be easily obtained. In any case, improved understanding of suprathermal electron production and transport is necessary.

VII. Sub-kilovolt X-ray Emission

We have performed extensive measurements of the time-dependence of sub-keV x-ray emission using a streak camera with time resolution of about 15 ps.[26] This allows observation of plasma heating and cooling processes in more detail than has been possible heretofor. Fig. 6 shows the observed emission-power time-dependence for three gold disk irradiations at 3×10^{14} W/cm^2, 25 J, 600 ps using 0.53 μm wavelength light. The rise- and fall- times are reproducible to within about 10%. We note that the rise-time corresponds quite closely to that of the incident laser pulse, whereas the fall-time is longer, since the plasma continues to radiate the absorbed energy as it cools. The corresponding results from LASNEX simulations are overlayed with arbitrary time and peak-power normalizations. Agreement is good to about 20%, with the calculated emission time somewhat longer than that measured, paritcularly for the low energy (100-200 eV) carbon-filtered channel.

The emission-time measurements show two systematic trends which are also seen in the LASNEX simulations. First, as shown in Fig. 7a, the radiated emission power FWHM decreases at increasing sub-keV photon energies. This is expected for a cooling, roughly-equilibrium plasma. Second, as shown in Fig. 7b, the radiation emission FWHM increases with increasing irradiation intensity. The LASNEX calculations track this trend. However, the result is rather subtle. The code shows that the dominant cooling processes are radiation and hydrodynamic expansion, and that the ratio of these cooling processes shifts from 2:1 at 3 X 10^{13} W/cm^2 to 1:2 at 2 X 10^{15} W/cm^2. The small shift in net cooling time results from the differences between these two strong, but nearly-compensating effects, and the somewhat weaker, but uncompensated effect of electron conduction cooling. With this complexity, the small quantitative discrepancy is less remarkable than the surprisingly good scaling.

The broad-band spectrum[1] of sub-keV x-rays emitted at 60° to the target normal is shown in Fig. 8 for 0.53 μm irradiations of gold disk targets at 3 X 10^{14} W/cm^2, 25 J, 600 ps. The spectrum was obtained by temporal-integration and spectral-unfold of the K- and L-edge-filtered 10-channel Dante-T x-ray-diode detector system. At the detected resolution, the spectrum is quite similar to that observed in previous 1.06 μm irradiations.[5] The LASNEX calculation plotted in Fig. 8 yields closely corresponding spectral shape and fluence. The calculation shows significant contribution to the emission around 0.8 keV from the broad group of N-shell line transitions which are excited in partially stripped gold at ~200 ev temperatures.

In order to determine the total sub-keV x-ray conversion efficiency, we have observed the emission at several angles with respect to the disk normal by using several detectors and three angles of incidence.[1] Two examples of measured angular distributions are shown in Fig. 9 for gold disk irradiations at 0.53 μm wavelength, with intensities of 3 X 10^{14} W/cm^2 and ~4 X 10^{15} W/cm^2. The temporally- and spectrally- integrated fluence is plotted as a function of the cosine of the angle β_n between the detector and the target normal. The angles of incidence employed were less than 30° to ensure that tilting the target modified the emission pattern as little as possible.

The LASNEX-calculated angular distributions are shown in Fig. 9 for comparison. Both the (2-D) calulated and measured angular distributions are flatter at ~4 X 10^{15} W/cm^2 than at 3 X 10^{14} W/cm^2. This occurs because the smaller (30-50 μm) spot diameter employed at ~4 X 10^{15} W/cm^2 makes the emitting region diameter comparable to its thickness (calculated to be 50 μm at this intensity). At 3 X 10^{14} W/cm^2, the (150 μm) spot diameter is considerably larger than the time-integrated emission region thickness, yielding a more strongly peaked emission pattern.

Finally, we integrate over the angular distribution to obtain the total energy emitted in x-rays above 0.1 keV. The results are plotted in Fig. 10 for titanium and gold disks, normalized by the energy absorbed in each case. We have estimated the absorptions for the titanium points by interpolating the measured absorptions for CH and

Au, and included the additional uncertainty in the conversion efficiency error bars. The calculated x-ray conversion efficiencies are seen to agree well with the measured values, except for the 3 X 10^{13} W/cm^2 gold irradiations. In general, the conversion efficiency increases with increasing target Z and decreasing intensity. These trends indicate generally improved conversion efficiency as the plasma conditions become more collisional.

The discrepancy between calculated and measured conversion efficiency for the 0.53 μm, 3 X 10^{13} W/cm^2 irradiations is quite interesting and has received considerable attention in the analysis. Numerically these calulations appear to be quite sound. Comparing the simulations further with the experiments, we find most of the observed features of the 3 X 10^{13} W/cm^2 irradiations to be in close correspondence with calculations. For example, the absorption characteristics, the sub-keV (broad-band) x-ray spectrum, and the sub-keV x-ray temporal- and spatial- distributions all appear to be nominal. One suggestive clue has been found: the observed 2.5 keV M-line emission drops by a factor of 5 between 3 X 10^{14} W/cm^2 and 3 X 10^{13} W/cm^2. The calculated M-line yield drops only by a factor of 1.5. One possible source of this discrepancy is an overestimate of the ionization state of gold for the 3 X 10^{13} W/cm^2 calculations. This could also affect the total x-ray conversion efficiency. We will investigate this area further.

We may draw on related 1.06 μm experiments to obtain a rough idea of the wavelength-scaling of the x-ray conversion efficiency. Earlier

1.06 μm experiments[5] with slightly different parameters measured the x-ray conversion efficiency somewhat more crudely at 3 X 10^{14} W/cm^2, 400 J, 900 ps and obtained about 33%, compared with 52 ± 15% for the current 0.53 μm experiments at 3 X 10^{14} W/cm^2, 25 J, 600 ps. Although considerable refinement is expected in the wavelength-scaling results, we feel justified in concluding that the x-ray conversion efficiency does increase as the laser wavelength decreases, at least qualitatively in accord with predictions.

VIII. Role of Electron Conduction

As discussed at the outset, electron conduction carries the energy from the laser deposition region near the critical density into the higher density plasma. Thus in low-Z plasmas, it determines the mass ablation rate and the ablation pressure, while in high-Z plasmas, it delivers the absorbed energy to the region where radiative processes occur strongly. In general, the corona density- and temperature- profiles depend fairly sensitively on the electron transport, so the laser-plasma interactions are affected by the transport coefficients.

For the LASNEX calculations presented in this report, we have utilized inhibited thermal transport with a flux-limit paramter of f_t = 0.03, which represents "anomalous" inhibition by a factor of ~10 below "classical" expectations. This yields the best over-all agreement with the current 0.53 μm experiments for both low- and high-Z targets.

We present in Table 2 some comparisons of calculations performed with and without inhibited thermal transport. Many aspects of the simulations diverge from experimental results when transport is not inhibited. We find that without thermal transport inhibition, the absorption calculated is generally too high, even when all non-linear absorption reductions are taken into account. Further, the sub-keV x-ray conversion efficiencies calculated for mid- and high-Z targets at high intensity are too high. However, a few aspects of the simulations improve with uninhibited transport. For example, calculations without inhibition do not exhibit the excessive mid-energy x-ray emission which is seen in the inhibited-conduction modeling.

On balance, the model with thermal transport inhibition provides better agreement with the data. We emphasize that inference of electron transport from general disk irradiations such as the present experiments is somewhat uncertain. The convolution of many physical effects makes the inference of electron transport coefficients uncertain, especially for the high-Z targets whe.e the atomic physics and radiative transport models are important. Experiments specifically designed to determine the behavior of electron transport at 0.35 μm wavelength using layered targets have been designed and are in progress.[27]

IX. Summary

We have presented an overview of the results of wavelength-scaling experiments irradiating Be-, CH-, Ti-, and Au- disk targets with 0.53 μm light in 25 J, 600 ps pulses, and spanning the intensity regime of 3 X 10^{13} W/cm^2 to ~4 X 10^{15} W/cm^2.

We find efficient absorption of the light, with intensity- and Z-scaling which matches expectations for strong collisional absorption by inverse bremsstrahlung The LASNEX absorption model including classical inverse bremsstrahlung and stimulated Brillouin scattering tracks the absorption to within 10-15%. For beryllium targets at the highest intensity, the absorption model requires either a resonance absorption "dump fraction" of about 30% or about 10-15% of additional absorption by some other means.

We observe some evidence that Brillouin scattering is operating at moderate levels in these experiments. Measured spectra for the back-reflected light show features which are difficult to interpret in detail, but which indicate that Brillouin scattering occurs in the higher-intensity irradiations. Large qualitative differences are observed between low-Z and high-Z back-reflected spectra. The highest calculated levels of Brillouin scattering are about 50% for the 2 X 10^{15} W/cm^2 beryllium disk case.

Stimulated Raman scattering is also occurring, although at very small ($<10^{-5}$) fractions of the incident laser energy. For the short

scale-length plasmas investigated here, these levels seem theoretically reasonable.

We have measured the intensity and Z-scaling of the hard x-ray fluence and slope. The simplest interpretation of the measured flux suggests that the suprathermal-electron population contains less than about 1% of the incident energy for all irradiation conditions employed. The slopes of the hard x-ray spectra at 2 X 10^{15} W/cm^2 are consistent with expectations for resonance absorption. LASNEX calculations can be brought into crude agreement with the measured hard x-ray fluence by assuming that about 3% of the light reaching the critical surface is resonantly absorbed. Improved theoretical understanding of the apparently-low levels of suprathermal populations is a matter for continuing study.

We have performed extensive temporal-, spectral-, and angular-observations of the sub-keV x-ray emission from titanium and gold disk targets. The x-ray emission time is slightly longer than the laser pulse width, with a slower fall-time than rise time, reflecting the plasma cool-down processes. The variation of emission time with intensity and photon frequency are tracked remarkably well by LASNEX simulations. Broad-band sub-keV spectral- and angular- distributions are similar to those calculated and seem adequately understood. We have observed efficient conversion of absorbed laser light into x-rays, using 0.53 μm light to irradiate gold disks. Our LASNEX calculations reproduce the Z- and intensity-scaling of the total x-ray conversion efficiency quite well, except for the gold, 3 X 10^{13} W/cm^2

point. Surprisingly, we measure lower conversion efficiency at 3×10^{13} W/cm^2 than at 3×10^{14} W/cm^2 in these 0.53 μm irradiations. *This remains to be investigated further.*

We obtain the best overall LASNEX simulations of these experiments using inhibited thermal transport ($f_\ell = 0.03$). However, the electron trasnport is tied closely enough to other physical processes that the deconvolution of electron transport coefficients from comparisons with the diagnostics is fairly uncertain. Other experiments employing, for example, layered targets, are required to more adequately isolate electron thermal transport.

With reference to similar 1.06 μm experiments, we can form some initial conclusions concerning wavelength-scaling. We find absorption increasing with decreasing wavelength. We infer suprathermal-electron temperatures at 2×10^{15} W/cm^2 which are consistent with expectations from resonance-absorption scaling. And we find that the efficiency of conversion of absorbed light into sub-keV x-rays increases as the wavelength decreases. More quantitative wavelength-scaling results will be forthcoming as the current ARGUS experiments continue.

Acknowledgements

The authors gratefully acknowledge the help and support of the many people who contributed in various ways to this work. We have appreciated support from J. L. Emmett, J. H. Nuckolls, H. G. Ahlstrom, and K. R. Manes.

We thank W. Hatcher and the target fabrication group for assistance. The Argus operations efforts of J. Hunt, W. Martin, J. Swain, G. Hermes, and others are appreciated. We thank L. N. Koppel and H. N. Kornblum for their contributions to the measurements and analysis.

Finally, we have benefitted from many discussions with colleagues, particularly D. S. Bailey, B. F. Lasinski, and G. B. Zimmerman.

REFERENCES

[1]E. M. Campbell, V. C. Rupert, W. C. Mead, R. E. Turner, C. E. Max, K. G. Estabrook, and F. Ze. 14th European Conf. on Laser Interaction with Matter, Palaiseau, France, Sept. 15-19,1980.

[2]G. B. Zimmerman, Lawrence Livermore National Laboratory Rpt. UCRL-75881 (1974); G. B. Zimmerman and W. L. Kruer, Comm. Plasma Phys. and Controlled Fusion 2, 85 (1975).

[3]R. A. Haas, W. C. Mead, W. L. Kruer, D. W. Phillion, H. N. Kornblum, J. D. Lindl, D. MacQuigg, V. C. Rupert, and K. G. Tirsell, Phys. Fluids 20, 322 (1977).

[4]H. D. Shay, R. A. Haas, W. L. Kruer, M. J. Boyle, D. W. Phillion, V. C. Rupert, H. N. Kornblum, F. Rainer, V. W. Slivinsky, L. N. Koppel, L. Richards, and K. G. Tirsell, Phys. Fluids 21, 1634 (1978).

[5]M. D. Rosen, D. W. Phillion, V. C. Rupert, W. C. Mead, W. L. Kruer, J. J. Thomson, H. N. Kornblum, V. W. Slivinsky, G. J. Caporaso, M. J. Boyle, and K. G. Tirsell, Phys. Fluids 22, 2020 (1979).

[6]A. B. Langdon, Phys. Rev. Lett. 44, 575 (1980).

[7]R. Faehl and W. L. Kruer, Phys. Fluids 20, 55 (1977); W. M. Manheimer, Phys. Fluids 20, 265 (1977).

[8]E. J. Valeo and W. L. Kruer, Phys. Rev. Lett. 33, 750 (1974); J. M. Kindel, K. Lee, and E. L. Lindman, Phys. Rev. Lett. 34, 134 (1975).

[9]K. G. Estabrook, E. J. Valeo, and W. L. Kruer, Phys. Fluids 18, 1151 (1975).

[10]K. G. Estabrook and J. Harte, Lawrence Livermore National Laboratory Rpt. UCRL-82620 (1979).

[11]R. M. More and G. B. Zimmerman, "Improvements in the LASNEX Atomic-Physics Package", in Laser Program Annual Report ~1979, Lawrence Livermore National Laboratory Rpt. UCRL-500-21-79 (1980), p. 3-66.

[12]W. L. Kruer, Comm. Plasma Phys. and Controlled Fusion 5, 69 (1979).

[13]C. E. Max and K. G. Estabrook, Comm. Plasma Phys. and Controlled Fusion 5, 239 (1980).

[14]C. E. Max, C. F. McKee, and W. C. Mead, Phys. Fluids 23, 1620 (1980).

[15]M. D. Rosen, "High Z Disk Modeling", in Laser Program Annual Report ~1979, LLNL Rpt. UCRL-500-21-79 (1980), p. 3-2.

[16]F. Amiranoff, R. Benattar, R. Fabbro, E. Fabre, C. Garban, and M. Weinfeld, Bull. Amer. Phys. Soc. 24, 1054 (1979); C. Garban-Labaune, E. Fabre, R. Fabbro, F. Amiranoff, and M. Weinfeld, in Report d'Activite 1979, GRECO Interaction Laser-Matiere, Ecole Polytechnique (Palaiseau, France, 1979), pp. 64-86.

[17]E. M. Campbell, F. Ze, D. W. Phillion, and V. C. Rupert, "Preliminary $2\omega_0$ Results", in Laser Program Annual Report ~1979, LLNL Rpt. UCRL-500-21-79 (1980), p. 6-46.

[18]W. L. Kruer, K. G. Estabrook, B. F. Lasinski, and A. B. Langdon, Phys. Fluids 23, 1326 (1980); K. G. Estabrook, W. L. Kruer, and B. F. Lasinski, Phys. Rev. Lett. 45, 1399 (1980).

[19]B. F. Lasinski and A. B. Langdon, "Linear Theory of the $2\omega_{pe}$ Instability in Inhomogeneous Plasmas", in Laser Program Annual Report — 1977, LLNL Rpt. UCRL-50021-77 (1978), p. 4-49.

[20]E. M. Campbell, S. M. Lane, B. L. Pruett, and H. N. Kornblum, "High Energy X-Ray Measurements from Disks of Different Z", in Laser Program Annual Report ~1979, Lawrence Livermore National Laboratory Rpt. UCRL-500-21-79 (1980), p. 6-26.

[21]A. H. Compton and S. K. Allison, X-rays in Theory and Experiment, (N.Y., Van Nostrand, 1935).

[22]K. G. Estabrook, M. D. Rosen, W. L. Kruer, and J. H. Nuckolls, "The Effect of Reheating on Hot-Electron Temperature", in Laser Program Annual Report ~1979, Lawrence Livermore National Laboratory Rpt. UCRL-500-21-79 (1980), p. 3-25.

[23]M. D. Rosen and K. G. Estabrook, LLNL Rpt. UCRL-82280 (1979).

[24]D. L. Banner, W. C. Mead, E. M. Campbell, and W. L. Kruer, "Electron Transport Analysis Using Layered Slab Targets", in Laser Program Annual Report ~1979, Lawrence Livermore National Laboratory Rpt. UCRL-500-21-79 (1980), p. 6-12.

[25]J. R. Albritton, I. B. Bernstein, E. J. Valeo, and E. A. Williams, Phys. Rev. Lett. 39, 1536 (1977).

[26]G. L. Stradling, R. L. Kauffman, E. M. Campbell, M. D. Rosen, and W. C. Mead, Bull. Amer. Phys. Soc. 25, 885 (1980).

[27]W. C. Mead, E. M. Campbell, and F. Ze, "Proposed Layered-Slab Experiments for 3ω ARGUS", LLNL Memorandum, Aug. 20, 1980.

Table 1. Order-of-magnitude estimates of hot-electron populations derived from hard x-ray flux measurements. T_h is the "temperature" inferred from the slope of the x-ray spectrum, while f_h is the fraction of the incident laser energy contained in a Maxwellian electron distibution which could produce the observed x-ray flux. The estimate neglects hydrodynamic losses, which LASNEX shows to be a factor of 2-4.

Target material	Irradiation intensity (W/cm^2)	Photon requency range (keV)	T_h (keV)	f_h (%)
Be	$3x10^{14}$	24.-46.	7.0±0.7	~1.
Ti	$3x10^{14}$	24.-46.	6.4±1.5	~0.1
Au	$3x10^{14}$	46.-70.	12.±4.	~0.3
Be	$2x10^{15}$	24.-46.	9.3±1.5	~0.5
Ti	$2x10^{15}$	24.-46.	13.±6.	~0.5
Au	$2x10^{15}$	46.-70.	19.±7.	~0.1

Table 2. Comparison of LASNEX calculations using inhibited or classical thermal electron transport with 0.53 μm observations at 3 X10^{15} W/cm^2, 600 ps. We weight the x-ray conversion efficiency more heavily in inferring electron transport properties, since it depends fairly directly upon conduction into the dense plasma. The absorption depends upon many competing processes, so is less reliable in determining transport coefficients.

Quantity Mat'l	Experiment	LASNEX	
		Inhibited	Classical
Absorption (%)			
Be	35.±10.	22.[1]	44.[1]
Au	45.±10.	46.[1]	75.[2]
X-ray conv. eff. (%)			
Ti	17.± 7.	15.	34.
Au	33.±10.	35.	45.

[1]Value obtained using $f_d = 0.03$, as suggested by the measured hard x-ray fluxes. Using $f_d = 0.3$ would raise the calculated absorption by 5-10%.

[2]Value of f_d affects this calculated absorption value little.

FIGURE CAPTIONS

Figure 1. LASNEX wavelength-scaling predictions. Calculations performed pre-shot for gold-disk target irradiations at 3 X 10^{14} W/cm^2. Absorption fraction (E_{ABS}/E_{INC}) and x-ray conversion efficiency (E_{RAD}/E_{ABS}) increase while energy into suprathermal electrons decreases at shorter wavelengths. The fraction of the absorbed energy which produces suprathermal electrons (E_{HOT}/E_{ABS}) decreases at shorter wavelengths.

Figure 2. LASNEX calculated plasma profiles for gold disk target irradiated at 0.53 μm, 3 X 10^{14} W/cm^2, 25 J, and 600 ps. Steep density, temperature fronts form at the critical surface. X-ray emission peaks just inside critical.

Figure 3. Measured and calculated absorptions for 0.53 μm irradiations of beryllium and gold disk targets. The horizontal bars represent the 30-70% intensity spread on a given shot. This spread is larger than the uncertainty in determining the intensity. Absorption increases with decreasing intensity and increasing Z. LASNEX calculations with f_d = 0.03 indicate need for added 10-15% absorption for the 2 X10^{15} W/cm^2 Be case.

Figure 4. Measured high energy x-ray spectra for disk targets irradiated with 0.53 μm light, 25 J in 600 ps Gaussian pulses: (a) for gold disks at varying intensity; and (b) for disks of varying Z at 2 X 10^{15} W/cm^2.

Figure 5. Comparison of measured and calculated high-energy x-ray spectra for gold disks at 0.53 μm, 2 X 10^{15} W/cm^2, 25 J, 600 ps. The calculations were performed with f_d-values of 0.3, 0.03, and 0. Best fit occurs for f_d = 0.03, indicating small amounts of resonance absorption.

Figure 6. Sub-keV x-ray radiated power *vs.* time, measured and calculated: (a) for carbon-filtered channel (about 100-200 eV); and (b) for vanadium-filtered channel (about 200-500 eV). The rise-time corresponds to the laser pulse rise. The fall-time, which is longer, shows the rate of plasma cool-down.

Figure 7. Scaling of radiated sub-keV emission FWHM for 0.53 μm, 3 X 10^{14} W/cm^2, 25 J, 600 ps irradiations of gold disks: (a) as a function of photon frequency; and (b) as a function of intensity, for the iron-filtered channel (600-700 eV).

Figure 8. Broad-band, sub-keV spectrum emitted at 60° to the target normal for gold disks irradiated with 0.53 μm light at 3 X 10^{14} W/cm^2, 25 J, and 600 ps. Overall agreement with LASNEX calculation is good.

Figure 9. Measured and calculated sub-keV angular distributions for 0.53 μm, 25 J, 600 ps gold disk irradiations at: (a) 3 X 10^{14} W/cm^2; and (b) ~4 X 10^{15} W/cm^2. Distribution for ~4 X 10^{15} W/cm^2 is flatter, since, for this case, the emission region thickness is comparable to the diameter of the focal spot.

Figure 10. Measured and calculated x-ray conversion efficiency as a function of intensity for titanium and gold disks irradiated at 25 J, 600 ps with 0.53 μm light. Excellent agreement is seen except for the surprizingly low measured conversion efficiency for the 3 X 10^{13} W/cm^2 gold target irradiations.

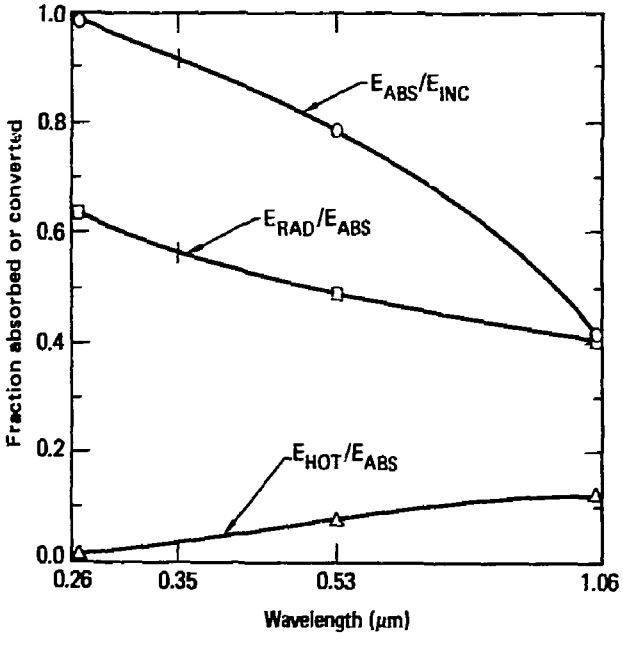
1.0
0.8
0.6
0.4
0.2
0.0
Fraction absorbed or converted
E_{ABS}/E_{INC}
E_{RAD}/E_{ABS}
E_{HOT}/E_{ABS}
0.26
0.35
0.53
1.06
Wavelength (μm)

Fig. 1

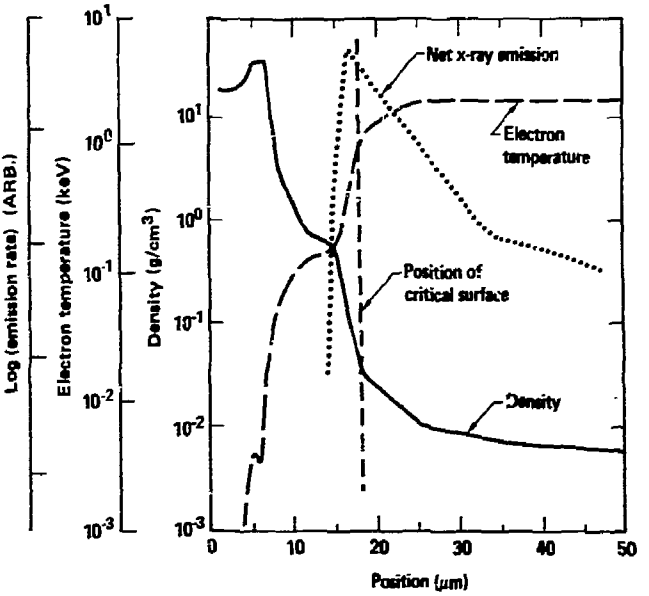
Log (emission rate) (ARB.)
Electron temperature (keV)
Density (g/cm³)
Net x-ray emission
Electron temperature
Position of critical surface
Density
Position (μm)
10¹
10⁰
10⁻¹
10⁻²
10⁻³
0
10
20
30
40
50

Fig. 2

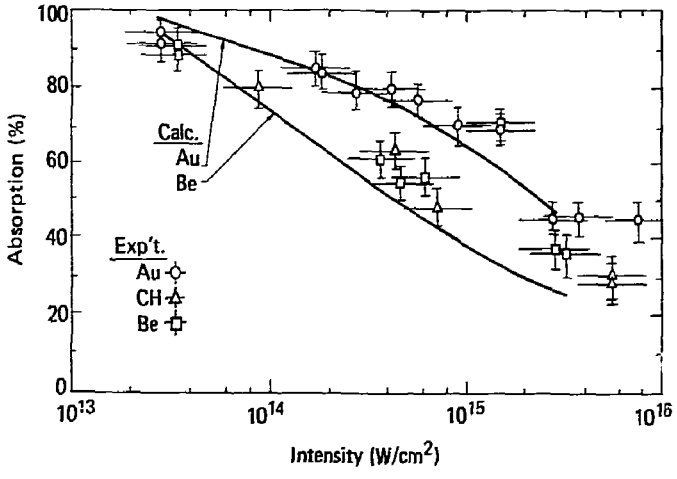
100
80
60
40
20
0
Absorption (%)
Calc.
Au
Be
Exp't.
Au
CH
Be
10^{13}
10^{14}
10^{15}
10^{16}
Intensity (W/cm^2)

Fig. 3

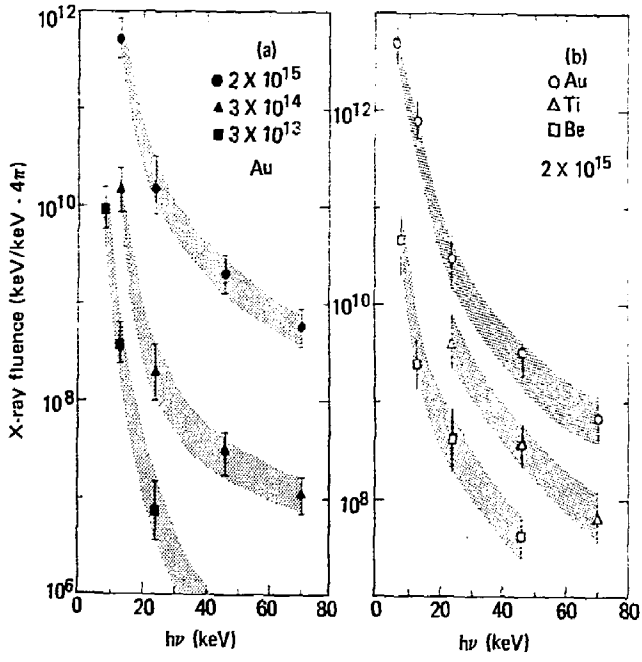
(a)
● 2 X 10^15
▲ 3 X 10^14
■ 3 X 10^13
Au
(b)
○ Au
△ Ti
□ Be
2 X 10^15
X-ray fluence (keV/keV · 4π)
hν (keV)
hν (keV)

Fig. 4

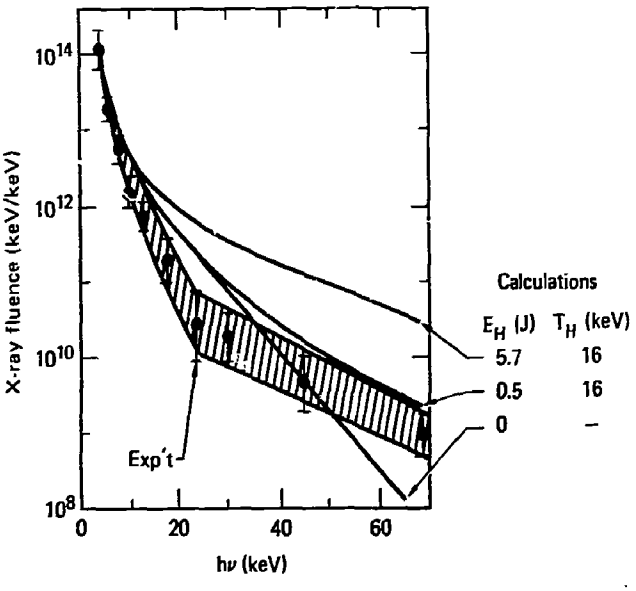
X-ray fluence (keV/keV)
10^{14}
10^{12}
10^{10}
10^{8}
0
20
40
60
hν (keV)
Exp't
Calculations
E_H (J) T_H (keV)
5.7 16
0.5 16
0 –

Fig. 5

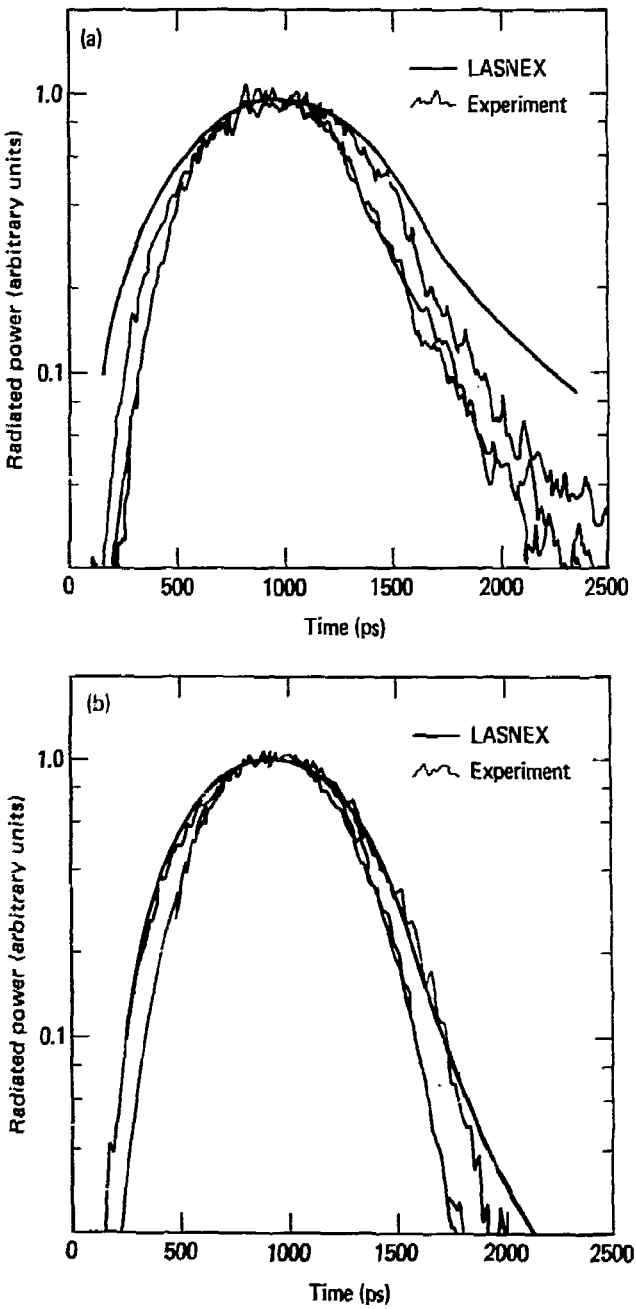
(a)
LASNEX
Experiment
1.0
0.1
Radiated power (arbitrary units)
0
500
1000
1500
2000
2500
Time (ps)
(b)
LASNEX
Experiment
1.0
0.1
Radiated power (arbitrary units)
0
500
1000
1500
2000
2500
Time (ps)

Fig. 6

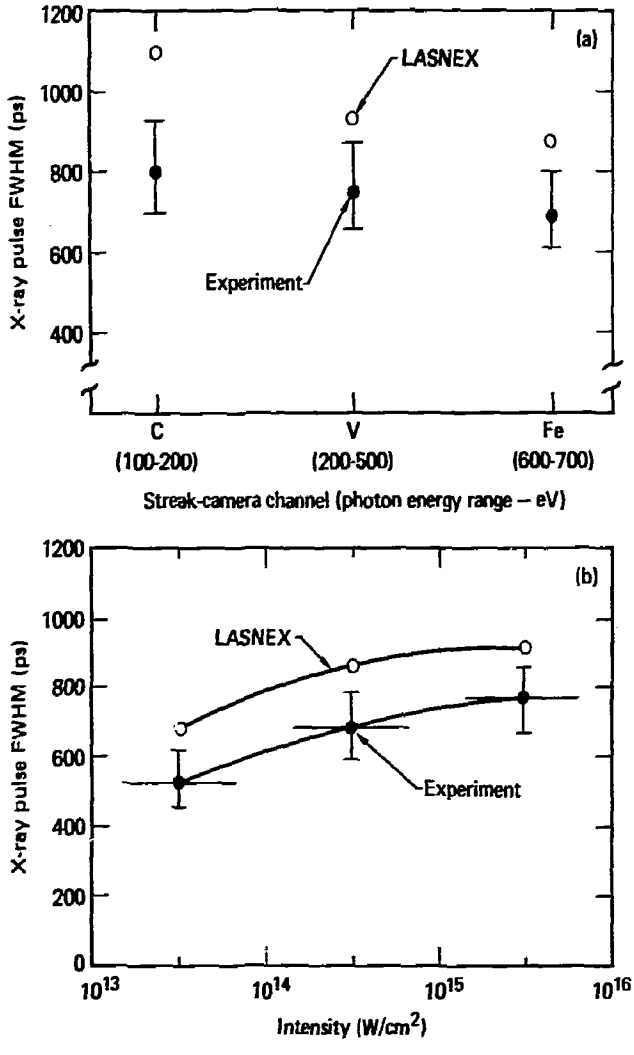
(a)
LASNEX
Experiment
X-ray pulse FWHM (ps)
1200
1000
800
600
400
C
(100-200)
V
(200-500)
Fe
(600-700)
Streak-camera channel (photon energy range – eV)
(b)
LASNEX
Experiment
X-ray pulse FWHM (ps)
1200
1000
800
600
400
200
0
10^{13}
10^{14}
10^{15}
10^{16}
Intensity (W/cm^2)

Fig. 7

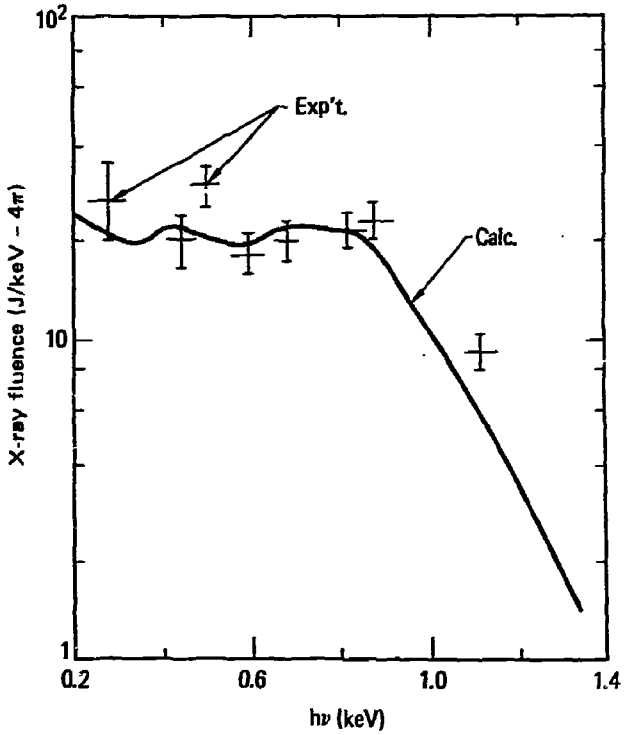

Fig. 3

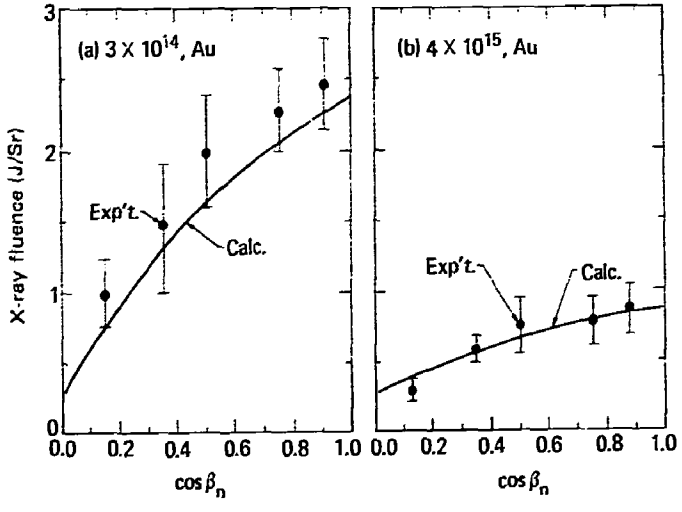
(a) 3 X 10^14, Au
(b) 4 X 10^15, Au
Exp't.
Calc.
Exp't.
Calc.
X-ray fluence (J/Sr)
0
1
2
3
0.0
0.2
0.4
0.6
0.8
1.0
cos β_n
cos β_n

Fig. 9

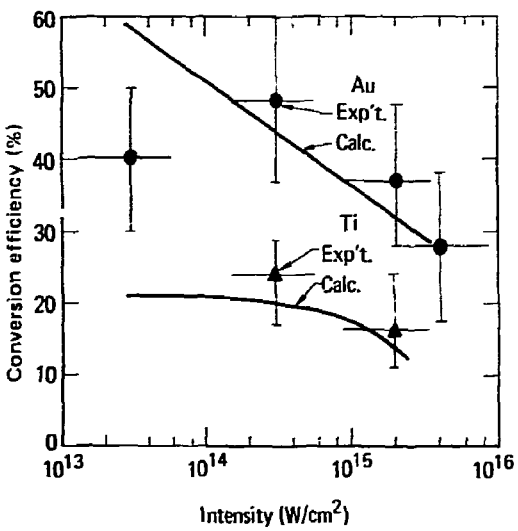
60
50
40
30
20
10
0
Conversion efficiency (%)
Au
Exp't.
Calc.
Ti
Exp't.
Calc.
10^{13}
10^{14}
10^{15}
10^{16}
Intensity (W/cm^2)

Fig. 10